ORIGINAL ARTICLE

Experimental and numerical study on transient elongational viscosity for PP/LDPE blends

Yasuhiko Otsuki[1] · Yoko Fujii[2] · Hiroko Sasaki[1] · Panitha Phulkerd[2] · Masayuki Yamaguchi[2]

Abstract

The transient uniaxial elongational viscosity for binary blends composed of polypropylene (PP) and low-density polyethylene (LDPE) was evaluated. A strain hardening behavior is detected for the blends, although LDPE is a dispersed phase. This behavior is attributed to LDPE dispersion deformation; the LDPE forms rigid fibers because of strain hardening. Rheological properties are calculated numerically by the Phan–Thien Tanner model by assuming a symmetric geometry with a periodic structure. Based on the simulation, we propose an appropriate LDPE to modify the processability of PP, for which the strain hardening in the elongational viscosity is required.

Introduction

Polymer blending is one of the most important technologies supporting the modern plastics industry and can improve product performance, such as mechanical and thermal properties. Rheological property modification is another target of polymer blending, enhancing the processability in various processing operations. The ability to increase the melt elasticity of a linear polymer is in strong demand in the industry. Several methods have been proposed to provide strain hardening in elongational viscosity, which is an important elastic property [1–10]. Among them, the simple addition of commercially available low-density polyethylene (LDPE) to isotactic polypropylene (PP) should be noted for potential industrial application [10]. In a previous study in which PP/LDPE blends were used, LDPE showed a slightly lower shear viscosity than PP, and it was suggested that the deformed LDPE droplets that were dispersed in the molten PP become rigid because of LDPE strain hardening during uniaxial elongational flow. Consequently, the blend behaved similar to a composite with rigid fibers, which led to a rapid increase in the elongational viscosity owing to the excess stress generation of a matrix between the fibrous dispersions [11–13]. Therefore, the viscosity ratio of the components, i.e., PP and LDPE, should have an important effect on the elongational viscosity of the blend systems, although this effect has not yet been revealed. One of the main purposes of this work is to clarify the effect of the viscosity ratio on the strain hardening behavior in the transient elongational viscosity for PP/LDPE blends. We also study the growth curves of elongational viscosity for PP/LDPE blends by numerical simulation based on the mechanism mentioned above. Because measurement data of elongational viscosity often contain experimental error, the results predicted by the numerical simulation should be considered seriously. In terms of PP processability, we propose an appropriate LDPE as a processing modifier based on the simulation.

To date, considerable theoretical work has been conducted on two-phase flow that consists of a matrix and dispersions in polymer blends. Most studies have focused on droplet deformation owing to the hydrodynamic force and droplet breakup and/or coalescence with consideration of the viscosity ratio, interfacial tension, capillary number, and flow pattern [14–21]. The simulation results have provided information on material design and the appropriate processing conditions to prepare polymer blends with fine dispersed droplets. In recent years, these research activities, such as the simulation of mechanical behaviors of

✉ Yasuhiko Otsuki
Yasuhiko.Otsuki@primepolymer.co.jp

✉ Masayuki Yamaguchi
m_yama@jaist.ac.jp

1 Packing and Industrial Materials Laboratory, Prime Polymer Co., Ltd., 3 Chigusa-Kaigan, Ichihara, Chiba 299-0108, Japan

2 School of Materials Science, Japan Advanced Institute of Science and Technology, 1-1 Asahidai, Nomi, Ishikawa 923-1292, Japan

individually dispersed droplets in a three-dimensional space [22] and an analysis of complicated three-dimensional droplet deformation [23], have advanced our understanding. However, numerical studies on the relationship between the structure of multiphase fluids and melt viscoelasticity have not been carried out extensively. In terms of elongational viscosity, several studies have been reported for a suspension system with rigid particles dispersed in a viscous fluid [24–26]. In these studies, flow simulations were performed for a suspension with a number of randomly dispersed rigid particles, and the simulations agreed well with the experimental data for planar elongational flow. If we consider the calculation cost and practical use, however, the calculation of a microstructural unit with one or two particles based on an assumption of the periodic existence of particles is preferred to predict the viscoelastic properties of a whole system. When rigid particles are arranged periodically under uniaxial elongational flow, however, they approach each other in the transversal direction relative to the flow, which leads to an unrealistic calculation result. Therefore, it is necessary to set rigid particles that are arranged randomly in the matrix. When particles are not rigid, they show a large deformation; in reality, this unrealistic structure will not occur even under a large deformation. Consequently, an approximation of the initial periodic structure will be kept until the final stage of deformation, which suggests that viscoelastic properties of a system that contains flexible particles can be predicted by a periodic local model.

Here, we carried out experiments using immiscible PP/LDPE blends with various viscosity ratios, in which LDPE particles were dispersed in the PP matrix. The experimental results obtained were compared with numerical simulations, which were performed by assuming a symmetric geometry with a periodic structure. The Lagrangian finite-element method with moving boundaries was used for isothermal creeping-flow simulation. The viscoelastic characteristics of the samples were described by the Phan–Thien Tanner (PTT) model with multiple relaxation modes. The contribution of interfacial tension was ignored because it is insignificant compared with the remarkable strain hardening of LDPE.

Experimental procedure

Materials

A propylene homopolymer (PP; Primepolymer, Tokyo, Japan) and three types of LDPE with different shear viscosities were used. The PP melt-mass flow rate was 3.0 g/10 min at 230 °C for 2.16 kg, and those of the LDPE were 3.7 for LDPE-L, 1.6 for LDPE-M, and 0.3 g/10 min for LDPE-H at 190 °C for 2.16 kg. LDPE-L and LDPE-M were produced by an autoclave reactor, whereas LDPE-H was produced by a tubular reactor. One of the LDPE samples, LDPE-M, and PP were used in our previous study [10].

The PP/LDPE blend samples (PP:LDPE = 70:30, weight ratio) were prepared by an internal batch mixer (Labo-Plastmill 10M100, Toyo Seiki Seisaku-sho, Tokyo, Japan) and by rotating the blades at 30 rpm at 190 °C for 3 min in the presence of 5000 ppm of thermal stabilizers, such as tris (2,4-di-tert-butylphenyl)phosphate (Irgafos168, Ciba, Bazel, Switzerland) and pentaerythritol tetrakis(3-(3,5-di-tert-butyl-4-hydroxyphenyl)propionate) (Irganox1010, Ciba). The blended samples were compressed into flat sheets at 190 °C for 5 min by using a compression-molding machine and quenched in the cooling unit.

Measurements

A cone-and-plate rheometer (AR2000ex, TA Instruments, New Castle, DW) was used to evaluate the frequency dependence of the shear storage modulus G' and loss modulus G'' at 190 °C. The cone angle was 4°, and its diameter was 25 mm. The growth curves of the transient uniaxial elongational viscosity were measured by the rotational rheometer equipped with a universal testing platform (SER2-G, Xpansion Instruments, Tallmadge, OH) at 190 °C. Rectangular 10-mm-wide, 15-mm-long, and 0.8-mm-thick samples were used for the measurements.

Numerical simulation

Governing equations

With consideration of the flow of a highly viscous fluid, ignoring the effects of inertia and gravity, and assuming that the fluid is isothermal and incompressible, the equation of motion and the equation of continuity are given by Eqs. (1) and (2), respectively.

$$-\nabla p + \nabla \cdot \boldsymbol{\tau} = \mathbf{0}, \tag{1}$$

$$\nabla \cdot \mathbf{v} = \mathbf{0}, \tag{2}$$

where p is the isotropic pressure, $\boldsymbol{\tau}$ is the stress tensor, and $\mathbf{v}$ is the velocity vector.

As the viscoelastic constitutive equation, the PTT model with multiple relaxation modes [27], represented by Eqs. (3), (4), and (5), was used, in which the stress-coefficient function $Y_i(\boldsymbol{\tau}_i)$ was expressed in exponential form:

$$Y_i(\boldsymbol{\tau}_i)\boldsymbol{\tau}_i + \lambda_i\left[\frac{\xi}{2}\overset{\Delta}{\boldsymbol{\tau}}_i + \left(1 - \frac{\xi}{2}\right)\overset{\triangledown}{\boldsymbol{\tau}}_i\right] = 2\eta_{0i}\mathbf{D}, \tag{3}$$

$$Y_i(\boldsymbol{\tau}_i) = \exp\left(\frac{\zeta}{G_i}\mathrm{tr}(\boldsymbol{\tau}_i)\right), \tag{4}$$

$$\boldsymbol{\tau} = \sum_{i=1}^{n} \boldsymbol{\tau}_i, \tag{5}$$

where $\mathbf{D}$ is the deformation velocity tensor. $\boldsymbol{\tau}_i$, λ_i, η_{0i}, and G_i are the stress tensor, relaxation time, zero shear viscosity, and relaxation modulus of the mode i, respectively. The superscripts $\triangle$ and $\triangledown$ represent the lower- and upper-convected time derivatives, respectively, and ξ and ζ are the nonlinear parameters used in the PTT model.

Numerical procedure

We previously reported flow analysis conducted during the stretching of foam with a moving boundary based on the Galerkin finite-element method [28]. In this study, the program was expanded to incorporate the dispersed phase as a viscoelastic fluid for the flow analysis. A Lagrange mesh was used, in which the positions of the nodes follow the mass point with the flow in the matrix and dispersed phases. The method used to calculate the flow field at time step $n+1$ based on that at time step n was as follows. If we assume that the coordinate value of a certain node is $\mathbf{X}$ and the velocity vector is $\mathbf{v}$, the coordinate value of the node at step $n+1$ was determined by the central difference method given by Eq. (6).

$$\mathbf{X}_{n+1} = \mathbf{X}_n + \frac{\mathbf{v}_{n+1} + \mathbf{v}_n}{2}\Delta t, \tag{6}$$

where subscripts n and $n+1$ indicate the values at the n and $n+1$ steps, respectively, and Δt is the time between consecutive steps.

To calculate the velocity field, a mesh that was composed of each node of $n+1$ steps was used to calculate Eq. (7) by the Galerkin FEM:

$$-\nabla p + 2\eta_r \nabla \cdot \mathbf{D}_{new} = -\nabla \cdot \boldsymbol{\tau} + 2\eta_r \nabla \cdot \mathbf{D}_{old}, \tag{7}$$

where the reference viscosity η_r was a calculation parameter that can be set arbitrarily. η_r was determined by the stress and velocity of the field [29]. The subscripts *old* and *new* represent the known and unknown values, respectively. In the iterative calculation, $\boldsymbol{\tau}$ and $\mathbf{D}$ on the right-hand side of Eq. (7) were substituted with the values obtained in the previous calculation, and the procedure to calculate new values of unknown variables on the left-hand side was repeated. In this analysis, a decoupled method was used, in which stress and velocity were solved separately and substituted alternately. Square elements with nine velocity nodes and four pressure nodes were used. To calculate the viscoelastic stress, a short time step was set according to the relaxation time, and the constitutive equation was integrated by the Runge–Kutta method with the stress of n steps as an initial value; hence, the stress value at the $n+1$ step was obtained.

In this multiphase flow analysis, we assumed no slippage at the interface. Therefore, the velocity is continuous at the interface, although other physical quantities, such as the velocity gradient, stress, and pressure, are discontinuous. For this reason, double nodes were arranged at the interface, in which different values of the physical quantities were used [30]. For the velocity analysis, however, the same nodes were shared for the matrix and dispersed phases to maintain the surface-force continuity. As described above, the prediction and correction of the velocity, the coordinates of the nodal point, and the stress were repeated until the calculated value converged, and then the process shifted to the next step (time).

Analytical model

By assuming the simplified initial structure shown in Fig. 1, the two-dimensional flow analysis was performed under the uniaxial elongational flow of two-phase materials. A local part was cut because of the periodicity and symmetry. Then, the unit cell in Fig. 1 was analyzed. By assuming a fine-grained hexagonal lattice of the dispersed phase as the initial morphology, a vertical rectangular model was set.

Figure 1 represents the model with a 30% dispersed phase. In the model with a 15% dispersed phase, the radius is reduced further in accordance with the volume fraction. This model allows dimensionless analysis, i.e., the absolute value of the domain size does not affect the analysis result because the surface tension is not considered. Here, a velocity boundary condition with a fixed amount was set in the x direction only on the right side of the analysis region, and the velocities in the direction perpendicular to the boundary plane along the x- and y-axes were set to zero. Because the x direction velocity on the right side of the analysis area was set, the Hencky strain rate $\dot{\varepsilon}_H$ of the field was a constant. As a result, the boundary moved with an exponential function. A two-dimensional flow analysis was performed by assuming that the physical quantities were constants in the depth direction z, and a compression strain rate of $\dot{\varepsilon}_H/2$ was set uniformly in the z direction. Therefore, the field deformation became uniaxial elongation. At the boundary of the upper side of the analysis area, the velocity in the y direction was set to be unknown, but the values were the same in this plane. Because incompressibility was assumed, the velocity was calculated (the elongational strain rate in the y direction was $-\dot{\varepsilon}_H/2$). For the FEM model, as shown in the figure on the right (Fig. 1), a mesh with 975 nodes and 216 elements was constructed. For the time step in the unsteady analysis, the time until the Hencky strain

**Fig. 1** Simplified two-dimensional model of two-phase elongational flow
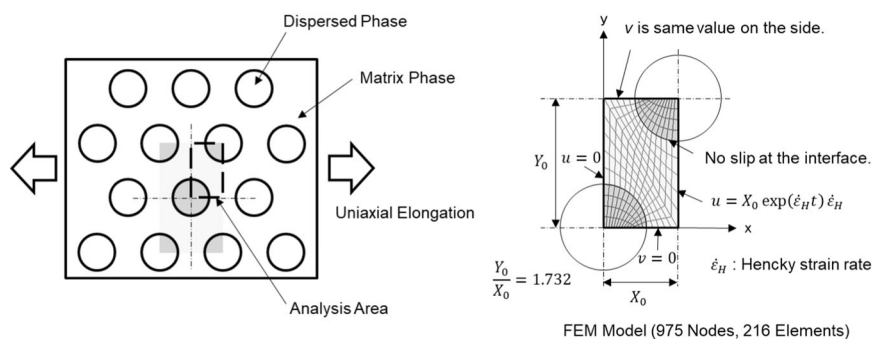
reached six was divided into 3000 steps for each elongational strain rate. A calculation of the elongational viscosity was obtained by dividing the average value of the normal stress difference in the y direction by the elongational strain rate. The inhomogeneity in the x direction was considered, and the elongational viscosity was calculated by dividing the average value of the normal stress differences across the whole analysis region by the elongational strain rate. As a test analysis of the FEM simulation, the elongational viscosity was calculated by setting the same viscoelastic characteristics for the matrix and dispersed phases, and this viscosity was compared with the elongational viscosity of the single material that was calculated directly from the constitutive equation. We confirmed that both methods gave the same results, which shows that the simulation method is reliable.

Results and discussion

Rheological properties of pure polymers

Figure 2 shows the oscillatory shear moduli, such as the storage modulus G'' and loss modulus G'', as a function of angular frequency ω for the pure samples at 190 °C. As shown in the figure, the oscillatory moduli of LDPE-H are higher than those of PP, whereas LDPE-L has lower moduli. The loss moduli of LDPE-M are slightly lower than those of PP. The relaxation spectra that were used for the simulation are estimated from the experimental data, as shown by the solid (G') and dotted (G'') lines.

Transient elongational viscosities for PP, LDPE-L, and LDPE-H are shown in Fig. 3. The data for LDPE-M were shown elsewhere [10]. The strain hardening behavior is detected as a steep slope for LDPE-L; a similar behavior is detected for LDPE-M. In contrast, LDPE-H shows weak strain hardening, i.e., a gentle slope, which is presumed to be attributed to the difference in the branch structure. Because LDPE-H is produced in a tubular reactor, the long-chain branch structure is not well-developed compared with that of the other LDPE samples, which were produced by an
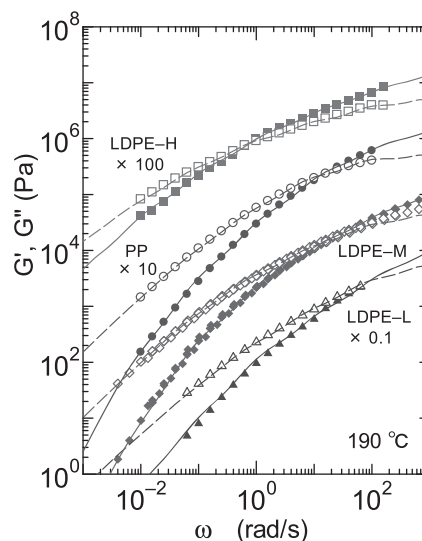

Fig. 2 Experimental (symbols) and calculated (lines) results of the frequency dependence of the shear storage modulus G''(closed symbols and solid lines) and loss modulus G'' (open symbols and dotted lines) for PP (circles), LDPE-L (triangles), LDPE-M (diamonds), and LDPE-H (squares) at 190 °C. The vertical axes were shifted

autoclave reactor [31–33]. The elongational viscosities of LDPE-L are lower than those of the pure PP at the beginning of the elongational flow (short time/strain region) and increase rapidly with time/strain. Finally, they exceed the values of the pure PP owing to the strain hardening. For LDPE-H, the elongational viscosities are higher than those of the pure PP from the beginning of the stretching.

The values calculated using the Runge–Kutta method that are derived directly from the PTT constitutive equation are also shown in Fig. 3 by the solid lines. It is found that the experimental data can be predicted successfully. The nonlinear viscoelastic parameters used in the simulations, such as ξ and ζ, are summarized in Table 1 with the relaxation spectra calculated from the linear viscoelasticity.

Uniaxial elongational viscosity of blends

As reported previously [10], PP/LDPE-M (70/30) and (85/15) showed a marked strain hardening behavior, with the
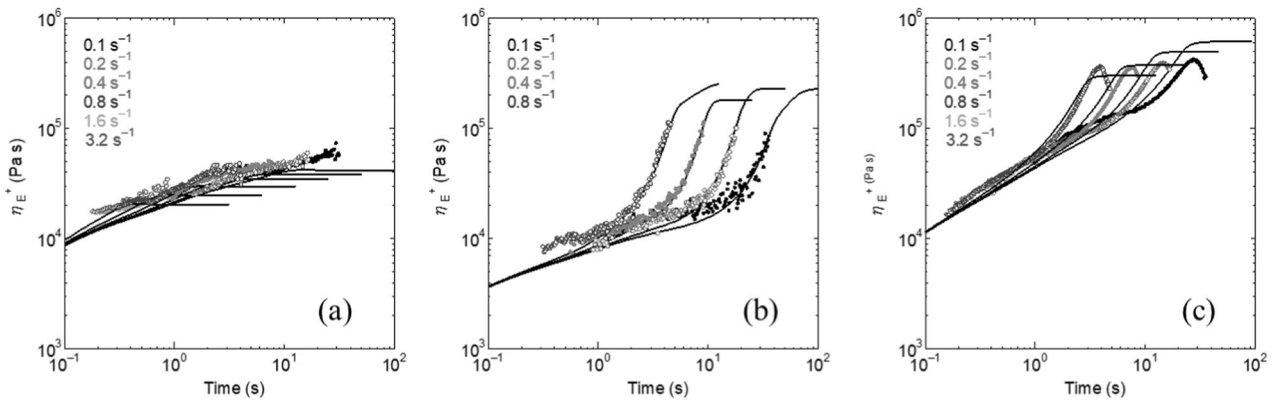
Fig. 3 Transient elongational viscosity with time at various Hencky strain rates at 190 °C for **a** PP, **b** LDPE-L, and **c** LDPE-H. The experimental data are shown as circles, and the solid lines represent the calculated values

Table 1 Relaxation spectra and PTT model parameters

λ (s)	G (Pa)			
	PP	LDPE-L	LDPE-M	LDPE-H
0.001	90,000	100,000	80,000	90,000
0.01	62,000	38,000	40,000	53,000
0.1	26,000	8600	14,000	26,000
1	4800	1800	3600	11,500
10	520	150	400	3200
100	20	10	8	600
1000	–	–	–	80
PTT model parameters				
ξ	0.12	0.15	0.15	0.15
ζ	0.5	0.005	0.005	0.08

behavior being intense for PP/LDPE-M (70/30). The calculated transient elongational viscosities η_E^+ are compared with the experimental data in Fig. 4 with those of other blends that contain low-viscosity LDPE-L and high-viscosity LDPE-H. The contributions of PP and LDPE to the elongational viscosity, calculated from the stress distribution generated in the two materials, are also indicated in the figure. First, both blend samples, i.e., PP/LDPE-L (70/30) and PP/LDPE-H (70/30), show a clear strain hardening behavior, which is similar to the case of the PP/LDPE-M blends. Second, it is confirmed that the calculation predicts the results.

When uniaxial elongational flow is applied to a blend having a sea-island structure with soft dispersion, the spherical dispersed droplets are elongated relative to the flow direction and assume a prolonged shape. As a result of this elongation, it eventually becomes necessary to take the interaction between these dispersed droplets into consideration. If this situation is strictly and numerically analyzed using a single domain, the two-dimensional axisymmetric problem occurs, and therefore, a three-

dimensional analysis is required. In the present study, however, this phenomenon is approximated by using a 2D rectangular coordinate system with sheet-like or ribbon-like dispersed (2D) droplets. Although the error caused by this approximation will be evaluated in the near future compared with the exact 3D model, it is expected that similar results are obtained by both models for the deformation mode and the growth of stress balance around the dispersed droplets. In fact, it was confirmed that the calculation of the approximated model successfully predicts the experimental data of the uniaxial elongational viscosities, as shown in Fig. 4, suggesting that this model is practically effective.

Here, the transient elongational viscosity of the blend material is estimated by a simple mixing rule and compared with the calculation result of the FEM analysis. Assuming the affine deformation of the dispersed phase, the transient viscosity of the mixture can be estimated by the following simple equation:

$$\eta_E^+(t, \dot{\varepsilon}_H) = \phi_c \eta_{Ec}^+(t, \dot{\varepsilon}_H) + \phi_d \eta_{Ed}^+(t, \dot{\varepsilon}_H), \qquad (8)$$

where η_E^+, η_{Ec}^+, and η_{Ed}^+ are the elongational viscosities of the mixture, continuous phase, and dispersed phase, respectively, and ϕ_c and ϕ_d are the volume fractions of the continuous and dispersed phases, respectively.

The elongational viscosity of the mixture was estimated by Eq. (8) using the calculated elongational viscosities of the single materials. As shown in Fig. 5, it was found that similar results to those of the FEM calculation were obtained for PP/LDPE-M, suggesting that the simple mixing rule is effective when the constituent materials show similar viscosities. However, differences appear for the other blends. When the dispersed phase has lower viscosity, i.e., PP/LDPE-L, the strain hardening occurs earlier for the FEM simulation. For the blend system, the internal strain of the dispersed droplets develops more quickly than the external strain, as mentioned later in the discussion on structure change. When the dispersed phase has a higher

Fig. 4 Transient elongational viscosity η_E^+ with time at various Hencky strain rates at 190 °C for **a** PP/LDPE-M (85/15), **b** PP/LDPE-M (70/30), **c** PP/LDPE-L (70/30), and **d** PP/LDPE-H (70/30). The solid lines represent the numerical results. The contributions of the stress generated in PP (dotted lines) and LDPE (dashed lines) are also indicated
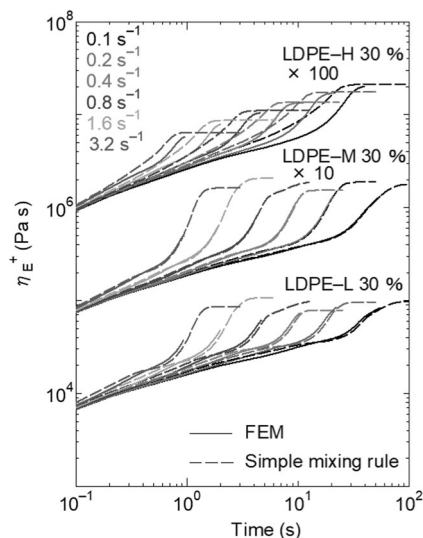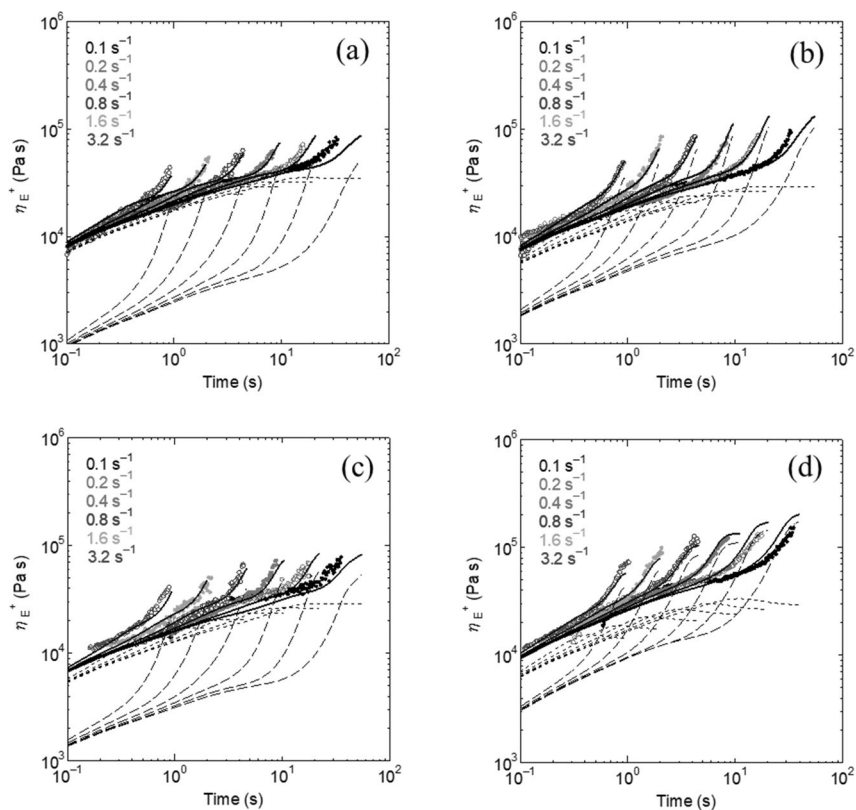
Fig. 5 Comparison of elongational viscosities predicted by the finite-element method (solid lines) and by the simple mixing rule (dashed lines)

viscosity, i.e., PP/LDPE-H, in contrast, the deformation of the dispersed droplets does not catch up with the external strain. Consequently, the strain hardening occurs over a longer time (larger strain) than required by the result obtained by the simple mixing rule. Furthermore, the

viscosity levels in the strain hardening region are considerably lower than those obtained by the simple mixing rule. This result is attributed to the low aspect ratio of dispersed LDPE-H. Batchelor [11] and Mewis and Metzner [12] clarified that the enhancement of the elongational viscosity by fiber addition is pronounced, with an increase in the fiber aspect ratio.

The contribution of the continuous phase to the elongational viscosity for the blends increases in the final stage in each system, as shown in Fig. 4. This increase indicates that there is indeed an effect of nonaffine deformation of the continuous phase, i.e., a higher elongation strain rate and/or higher normal stress difference in some area. Figure 4 also indicates that the contribution of the dispersed phase increases rapidly in the large deformation area, suggesting that the dispersed phase eventually shows pseudo affine deformation.

To clarify the difference in the strain hardening for the blend samples quantitatively, the calculated values of the blends with 30% LDPE are shown in Fig. 6, along with those of the pure components, i.e., PP and LDPE. Compared with PP/LDPE-H, both PP/LDPE-M and PP/LDPE-L show strain hardening in the long time (large strain) region, i.e., the strain hardening is delayed. This result is reasonable because a large strain is required for LDPE-L and LDPE-M to show a higher elongational viscosity than that of PP,

Fig. 6 Calculated elongational viscosity of PP, LDPE, and the blend with 30% LDPE. (Left) $\dot{\varepsilon}_H = 0.8\,\mathrm{s}^{-1}$ and (right) $\dot{\varepsilon}_H = 0.1\,\mathrm{s}^{-1}$
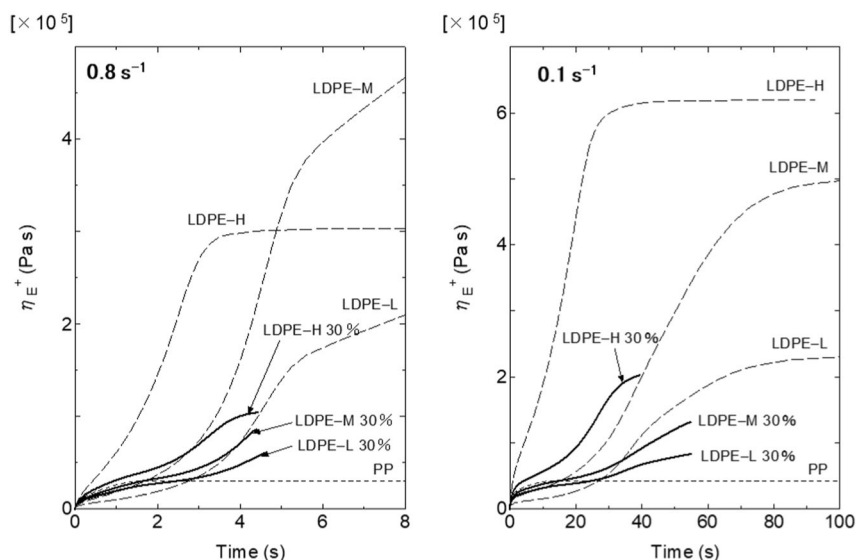
Fig. 7 Numerical results of structure development under uniaxial elongational flow for blends with 30% LDPE
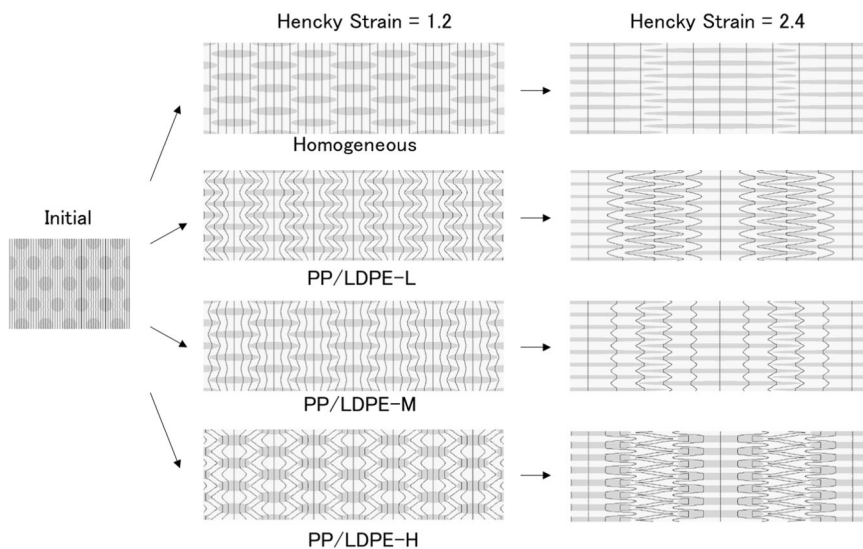
although the difference in onset of strain hardening between PP/LDPE-M and PP/LDPE-L is minimal, as will be discussed later. In contrast, strain hardening occurs in the short time region for the blend with LDPE-H, owing to the prompt stress growth of LDPE-H. Even though strain hardening of the dispersed droplets in PP/LDPE-H is delayed relative to that of LDPE-H alone, the strain hardening still occurs in the shorter time region compared with the other blends.

Development of morphology and stress distribution

As commented previously, the shape of the dispersed phase has a strong impact on the rheological behavior under elongational flow. Therefore, the structure development of

the blends containing 30% LDPE is calculated. Figure 7 shows the structures during stretching at Hencky strains ε_H of 1.2 and 2.4.

In the figure, longitudinal lines in the initial state are inserted periodically to comprehend the deformation easily. Furthermore, the structures are magnified to see the lines clearly at Hencky strains of 1.2 and 2.4. For the homogeneous material, in which the continuous and dispersed phases are the same substance, both phases deform in the same way. Therefore, the lines remain straight with increasing distance as the deformation progresses. When the dispersed phase shows a viscoelasticity different from that of the continuous phase, the lines become distorted. For PP/LDPE-L, the dispersions deform more rapidly than the external deformation in the early stage of elongation, which
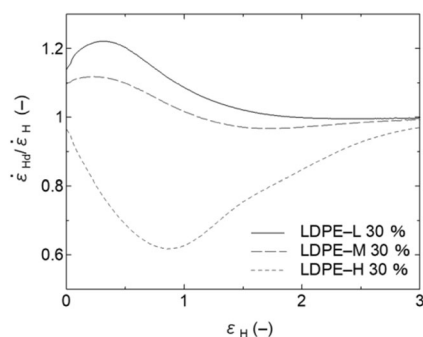
Fig. 8 Ratio of the Hencky strain rate of the dispersion to the external strain rate, $\dot{\varepsilon}_{Hd}/\dot{\varepsilon}_H$, as a function of the external strain ε_H for PP/LDPE (70/30) at $\dot{\varepsilon}_H = 0.8$ s^{-1}

Fig. 9 Distributions of tensile stress at the center of the dispersed phase and shear stress at the surface of the dispersed phase at $\varepsilon_H = 1.8$ and 2.4 during elongation flow at $\dot{\varepsilon}_H = 0.8$ s^{-1} for PP/LDPE-M (70/30)

promptly leads to prolonged droplets. This structure development of blends with a sea-island morphology has been reported previously by advanced research groups [15, 19, 34]. Similarly, the LDPE-M dispersions, which show a slightly lower viscosity than that of the continuous PP in the short time region, deform more than the external strain, although their deformation is smaller than that of the LDPE-L. Because LDPE-L shows a larger deformation in the blend, the onset strain needed to show strain hardening is not so different from that for PP/LDPE-M (Fig. 6). In contrast, the LDPE-H deformation is delayed because of its higher viscosity than the continuous PP. Because the deformation of the dispersed phase cannot catch up with the continuous one for PP/LDPE-H, the LDPE-H droplets do not overlap each other even under a large deformation, and thus, nonuniformity appears in the width direction. In this analysis model, the periodic configuration is assumed, and the dispersed droplets are arranged straight vertically. Since the dispersed phase is not so hard for PP/LDPE-H, the elongational viscosity could be predicted by averaging the stress in the width direction. However, if the viscosity of a dispersed phase is too high to be undeformable during elongational flow, i.e., dispersed particles behave as a rigid body similar to inorganic fillers, this analytical model will not be applicable.

Figure 8 shows the ratio of the Hencky strain rate of a dispersion $\dot{\varepsilon}_{Hd}$ to the external strain rate $\dot{\varepsilon}_H$, i.e., $\dot{\varepsilon}_{Hd}/\dot{\varepsilon}_H$, as a function of the external strain for the blends with 30% LDPE. The strain rate of a dispersion is determined by $(dR_1/dt)/R_1$, where R_1 is the major radius of the dispersion.

Figure 8 shows that the effect of the LDPE species appears in the early stage of the elongational flow. Furthermore, the direction of the deviation, i.e., upper (larger than unity) or lower (smaller than unity), is determined by the viscosity ratio of PP to LDPE. It is interesting to note that the ratio of the blend with LDPE-M is larger than unity initially and smaller than unity beyond a strain of 1.1, i.e., the dispersions act as long rigid fibers.
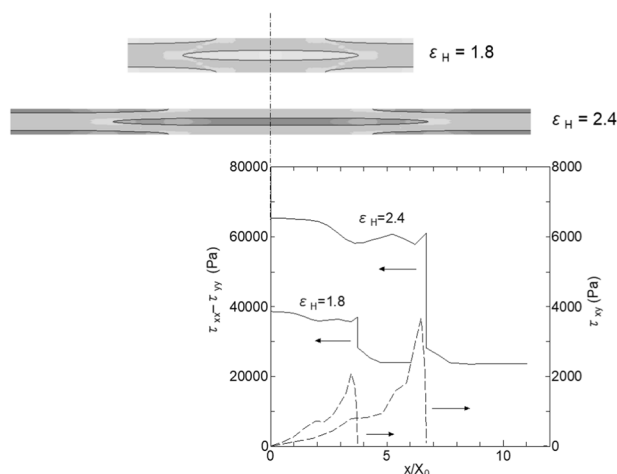
It is also found that the ratios of the strain rates, i.e., $\dot{\varepsilon}_{Hd}/\dot{\varepsilon}_H$, gradually approaches one for all blends, although the values in the initial stage are determined by the viscosity ratio of PP to LDPE. This result indicates that all systems approach affine deformation under a large deformation, which is prominent, especially for the blend systems with LDPE-L and LDPE-M. Therefore, the values predicted by the simple mixing rule were close to those of the FEM analysis, as shown in Fig. 5.

Figure 9 shows the distributions of shear stress τ_{xy} at the boundary surface of a dispersion and tensile stress $\tau_{xx} - \tau_{yy}$ at the center of a dispersion in the x direction during stretching at $\dot{\varepsilon}_H = 0.8$ s^{-1} for PP/LDPE-M (70/30). The shear stress shows that the maximum occurs at the end of the elliptical dispersion and decreases toward the center, which balances the tensile stress that is generated in the dispersion. With an increase in the aspect ratio of the dispersion, the shear stress, especially near the end parts of the dispersion, is enhanced significantly. Moreover, the elongational stress in the dispersion is high, as revealed by previous studies [35, 36]. As a result, the apparent elongational viscosity for the whole system is enhanced. This stress distribution was also confirmed in the elastic deformation analysis for a composite material with long cylindrical fibers [37, 38]. In the present system, however, a large elongational stress is detected for the whole LDPE dispersion, which is different from the stress distribution in the cylindrical fiber composite. This phenomenon occurs because the cross-sectional area of the dispersion decreases toward the end, which leads to a high elongational stress near the end [39].

It is found that the elongation stress acting on the dispersed phase is considerably higher than the shear stress at the surface of the dispersion. When the aspect ratio

increases, the interfacial area of the dispersed droplets increases greatly with the decrease in the vertical cross-sectional area. As a result, dispersed droplets with high viscosity can be deformed affinely. Figure 9 also shows that the shear stress is low near the center of the dispersed droplet. A similar situation was also detected for a composite system with long fibers, suggesting that the center area is affinely deformed. Although the strain hardening occurs in the dispersion under a large strain, the dispersion shows pseudo affine deformation following the external strain rate. Thus, high elongational stress develops in the dispersed phase, which directly contributes to the increase in the elongational viscosity of the blend. This situation is magnified with the increase in volume fraction of the dispersed phase.

The simulation result indicates that the elongational viscosity of the PP/LDPE blend systems can be controlled by the ratio of the elongational viscosities between PP and LDPE and the strain hardening behavior of LDPE. When the LDPE shows a lower viscosity, it turns into a fibrous shape promptly. Then, a steep increase in elongational viscosity, i.e., pronounced strain hardening, is provided for the blend after stretching to some degree, i.e., the strain hardening is delayed. When the strain hardening is required in the early stage of flow, e.g., reduction of the neck-in level at T-die extrusion, LDPE that has a slightly higher shear viscosity with marked strain hardening in the elongational viscosity is recommended. In the case of foaming, LDPE with a low shear viscosity would be recommended to achieve a large expansion ratio because the strain hardening occurs at a large strain.

Conclusions

The effect of LDPE addition on the rheological properties of PP under uniaxial elongational flow is investigated. The LDPE addition is found to provide strain hardening in the transient elongational viscosity for PP even though LDPE is the dispersed phase. Moreover, the experimental results are predicted by the numerical simulation by using the PTT model with multiple relaxation modes by assuming a symmetric geometry with a periodic structure. The transient elongational viscosity for pure LDPE determines the critical strain needed to exhibit strain hardening and the magnitude of strain hardening for the blends. When the shear viscosity of LDPE is lower than that of PP, the strain hardening appears later with a steep slope, where LDPE dispersions have a high aspect ratio. In contrast, the blend with LDPE with a higher viscosity shows strain hardening in the early stage of flow. These results obtained in this study will be useful in selecting an appropriate LDPE as a processing modifier for PP in real processing operations.

Compliance with ethical standards

References

1. Yamaguchi M, Miyata H. Strain hardening behavior in elongational viscosity for binary blends of linear polymer and cross-linked polymer. Polym. J. 2000;32:164–70.
2. Sugimoto M, Masubuchi T, Takimoto J, Koyama K. Melt rheology of polypropylene containing small amounts of high-molecular-weight chain. 2. Uniaxial and biaxial extensional flow. Macromolecules. 2001;34:6056–63.
3. Kurose T, Takahashi T, Sugimoto M, Taniguchi T, Koyama K. Uniaxial elongational viscosity of PC/ A small amount of PTFE blend. Nihon Reoroji Gakkaishi. 2005;33:173–82.
4. Yamaguchi M, Wakabayashi T. Rheological properties and processability of chemically modified poly(ethylene terephthalate-co-ethylene isophthalate). Adv. Polym. Technol. 2006;25: 236–41.
5. Mieda N, Yamaguchi M. Flow instability for binary blends of linear polyethylene and long-chain branched polyethylene. J. Non-Newtonian Fluid Mech. 2011;166:231–40.
6. Yokohara T, Nobukawa S, Yamaguchi M. Rheological properties of polymer composites with flexible fine fiber. J. Rheology. 2011;55:1205–18.
7. Yamaguchi M, Yokohara T, Ali MAB. Effect of flexible fibers on rheological properties of poly(lactic acid) composites under elongational flow. Nihon Reoroji Gakkaishi. 2013;41:129–35.
8. Siriprumpoonthum M, Nobukawa S, Satoh Y, Sasaki H, Yamaguchi M. Effect of thermal modification on rheological properties of polyethylene blends. J. Rheology. 2014;58:449–66.
9. Seemork J, Sako T, Ali MAB, Yamaguchi M. Rheological response under non-isothermal stretching for immiscible blends of isotactic polypropylene and acrylate polymer. J. Rheology. 2017;61:1–11.
10. Fujii Y, Nishikawa R, Phulkerd P, Yamaguchi M. Modifying the rheological properties of polypropylene under elongational flow by adding polyethylene. J. Rheology. 2019;63:11–18.
11. Batchelor GK. The stress generated in a non-dilute suspension of elongated particles by pure straining motion. J. Fluid Mech. 1971;1971:813–29.
12. Mewis J, Metzner AB. The rheological properties of suspensions of fibres in Newtonian fluids subjected to extensional deformations. J. Fluid Mech. 1974;62:593–600.
13. Laun HM. Orientation effects and rheology of short glass fiber-reinforced thermoplastics. Colloid Polym. Sci. 1984;262: 257–69.
14. Toose EM, Geurts BJ, Kuerten JMG. A boundary integral method for two-dimensional (non)-Newtonian drops in slow viscous flow. J. Non-Newtonian Fluid Mech. 1995;60:129–54.
15. Delaby I, Ernst B, Froelich D, Muller R. Droplet deformation in immiscible polymer blends during transient uniaxial elongational flow. Polym. Eng. Sci. 1996;36:1627–35.

16. Ramaswamy S, Leal LG. The deformation of a viscoelastic drop subjected to steady uniaxial extensional flow of a Newtonian fluid. J. Non-Newtonian Fluid Mech. 1999;85:127–63.

17. Ramaswamy S, Leal LG. The deformation of a Newtonian drop in the uniaxial extensional flow of a viscoelastic liquid. J. Non-Newtonian Fluid Mech. 1999;88:149–72.

18. Hooper RW, de Almeida VF, Macosko CW, Derby JJ. Transient polymeric drop extension and retraction in uniaxial extensional flows. J. Non-Newtonian Fluid Mech. 2001;98:141–68.

19. Cristini V, Hooper RW, Macosko CW, Simeone M, Guido S. A numerical and experimental investigation of lamellar blend morphologies. Ind. Eng. Chem. Res. 2002;41:6305–11.

20. Mukherjee S, Sarkar K. Effects of viscosity ratio on deformation of a viscoelastic drop in a Newtonian matrix under steady shear. J. Non-Newtonian Fluid Mech. 2009;160:104–12.

21. Cardinaels R, Afkhami S, Renardy Y, Moldenaers P. An experimental and numerical investigation of the dynamics of micro-confined droplets in systems with one viscoelastic phase. J. Non-Newtonian Fluid Mech. 2011;166:52–62.

22. Skartilien R, Sollum E, Akselsen A, Meakin P. Direct numerical simulation of surfactant-stabilized emulsions. Rheol. Acta. 2012;51:649–73.

23. Isbassarov D, Rosti ME, Ardekani MN, Sarabian M, Hormozi LB, Tammisola O. Computational modeling of multiphase viscoelastic and elastoviscoplastic flows. Int. J. Numerical Methods Fluids. 2018;88:521–43.

24. Hwang WR, Hulsen M. Direct numerical simulations of hard particle suspensions in planar elongational flow. J. Non-Newtonian Fluid Mech. 2006;136:167–78.

25. D'Avino G, Maffettone PL, Hulsen MA, Peters GWM. A numerical method for simulating concentrated rigid particle suspensions in an elongational flow using a fixed grid. J. Comp. Phys. 2007;226:688–711.

26. Ahamdi M, Harlen OG. A Lagrangian finite element method for simulation of a suspension under planar extensional flow. J. Comp. Phys. 2008;227:7543–60.

27. Phan-Thien N, Tanner RI. A new constitutive equation derived from network theory. J. Non-Newtonian Fluid Mech. 1977;2:353–65.

28. Otsuki Y, Umeda T, Tsunori R, Shinohara M. Viscoelastic simulation of deformation-induced bubble coalescence in foaming process. Nihon Reoroji Gakkaishi. 2005;33:9–16.

29. Otsuki Y, Kajiwara T, Funatsu K. Numerical simulations of annular extrudate swell using various types of viscoelastic models. Polym. Eng. Sci. 1999;39:1969–81.

30. Matsunaga K, Kajiwara T, Funatsu K. Numerical simulation of multi-layer flow for polymer melts—A study of the effect of viscoelasticity on interface shape of polymers within dies. Polym. Eng. Sci. 1998;38:1099–111.

31. Tackx P, Tacx JCJF. Chain architecture of LDPE as a function of molar mass using size exclusion chromatography and multi-angle laser light scattering (SEC-MALLS). Polymer. 1998;39:3109–13.

32. Yamaguchi M, Takahashi M. Rheological properties of low density polyethylenes produced by tubular and vessel processes. Polymer. 2001;42:8663–70.

33. Mieda N, Yamaguchi M. Anomalous rheological response for binary blends of linear polyethylene and long-chain branched polyethylene. Adv. Polym. Technol. 2007;26:173–81.

34. Levitt L, Macosko CW, Pearson SD. Influence of normal stress difference on polymer drop deformation. Polym. Eng. Sci. 1996;36:1647–55.

35. Goddard JD. Tensile stress contribution of flow-oriented slender particles in non-Newtonian fluids. J. Non-Newtonian Fluid Mech. 1976;1:1–17.

36. Pipes RB, Hearle JWS, Beaussart AJ, Sastry AM, Okine RK. A constitutive relation for the viscous flow of an oriented fiber assembly. J. Compos. Mater. 1991;25:1204–17.

37. Carrara AS, Mcgarry FJ. Matrix and interface stresses in a discontinuous fibre. composite model. J. Comp. Mat. 1968;2:222–43.

38. Harris, B, Engineering Composite Materials, 2nd ed. Leeds: Maney Publishing; 1999.

39. Goh KL, Mathias KJ, Aspden RM, Hukins DWH. Finite element analysis of the effect of fibre shape on stresses in an elastic fibre surrounded by a plastic matrix. J. Mater. Sci. 2000;35:2493–97.